

The absorption spectrum of D₂:
Ultrasensitive CRDS measurements of the (2-0) band near 1.7 μm
and accurate *ab initio* line list up to 24000 cm⁻¹

Samir Kassi ^a, Alain Campargue ^{a 1}, Krzysztof Pachucki ^b and Jacek Komasa ^c

^a Université Grenoble 1/CNRS, UMR5588 LIPhy Grenoble, F-38041, France

^b Faculty of Physics, University of Warsaw, Hoża 69, 00-681 Warsaw, Poland

^c Faculty of Chemistry, A. Mickiewicz University, Grunwaldzka 6, 60-780 Poznań, Poland

11th April 2012

Number of figures: 7

Number of Tables: 4

Running Head: *The absorption spectrum of D₂*

Keywords: *hydrogen; D2, deuterium, quadrupole transition, absorption spectroscopy, CRDS, spectroscopic database, nonadiabatic corrections, relativistic and QED effects*

¹ Corresponding author: Alain. Campargue@ujf-grenoble.fr

Abstract

Eleven very weak electric quadrupole transitions $Q(2)$, $Q(1)$, $S(0)$ - $S(8)$ of the first overtone band of D_2 have been measured by very high sensitivity CW-Cavity Ring Down Spectroscopy (CRDS) between 5850 and 6720 cm^{-1} . The noise equivalent absorption of the recordings is on the order of $\alpha_{min} \approx 3 \times 10^{-11} \text{ cm}^{-1}$. By averaging a high number of spectra, the noise level was lowered to $\alpha_{min} \approx 4 \times 10^{-12} \text{ cm}^{-1}$ in order to detect the $S(8)$ transition which is among the weakest transitions ever detected in laboratory experiments (line intensity on the order of $1.8 \times 10^{-31} \text{ cm/molecule}$). A Galatry profile was used to reproduce the measured line shape and derive the line strengths. The pressure shift and position at zero pressure limit were determined from recordings with pressures ranging between 10 and 750 Torr.

A highly accurate theoretical line list was constructed for pure D_2 at 296 K. The intensity threshold was fixed to a value of $1 \times 10^{-34} \text{ cm/molecule}$ at 296 K. The obtained line list is provided as Supplementary Material. It extends up to 24000 cm^{-1} and includes 201 transitions belonging to ten $\nu=0$ cold bands ($\nu=0-9$) and three $\nu=1$ hot bands ($\nu=1-3$). The energy levels include the relativistic and quantum electrodynamic corrections as well as the effects of the finite nuclear mass. The quadrupole transition moments are calculated using highly accurate adiabatic wave functions.

The CRDS line positions and intensities of the first overtone band are compared to the corresponding calculated values and to previous measurements of the $S(0)$ - $S(3)$ lines. The agreement between the CRDS and theoretical results is found within the claimed experimental uncertainties (on the order of $1 \times 10^{-3} \text{ cm}^{-1}$ and 2 % for the positions and intensities, respectively) while previous measurements showed important deviations for the line intensities.

1. INTRODUCTION

Although they have similar absorption spectra, much less laboratory observations are available for D_2 than for H_2 . D_2 has not yet been observed in outer space due to its very low abundance and lack of electric-dipole-allowed vibrational transitions. After the first laboratory detection from Raman spectra in 1935 [1,2], D_2 transitions have been observed and measured by several groups using electric quadrupole absorption spectroscopy [3], electric-field-induced spectroscopy [4] and Raman spectroscopy [5-12]. The observation of the Lyman and Werner bands of D_2 by Bredohl and Herzberg [13] resulted in a collection of dissociation energies for the D_2 bound rovibrational levels of the electronic ground state ($X^1\Sigma_g^+$). More recently, Gupta et al. reported line intensities for the first overtone band [14] and while Maddaloni et al. measured accurate line frequencies and intensities for the fundamental band by [15]. Moreover, the dissociation energy has been measured by Liu et al. with a 10^{-4} cm^{-1} accuracy [16]. On the other side, calculations of molecular hydrogen spectra progressed continuously since the original works by James and Coolidge in 1933 [17]. In a series of papers [18,19], Kolos and Wolniewicz predicted line positions and intensities for H_2 and its isotopologues with an accuracy which was at the state of the art at that time. More recently, the development of advanced computational techniques and of the quantum electrodynamic theory made possible theoretical predictions of all rovibrational levels of molecular hydrogen in its electronic ground state with an accuracy on the order of 10^{-3} cm^{-1} . Theoretically predicted dissociation energy [20] and para-ortho energy separation [21] of the lowest rotational levels were found in good agreement with experimental values [16]. The precision achieved in the calculations of the hydrogen spectrum [22, 23] gives an exceptional opportunity for a constructive interplay between theory and experiment. Once validated by the most accurate measurements, theoretical results can be used in spectral regions inaccessible for current experiments and supply data useful e.g. for the astrophysical search of molecular deuterium lines.

The objective of the present contribution is twofold: (i) new detection of transitions of the first overtone band of D_2 by high sensitivity CW-Cavity Ring Down Spectroscopy (CRDS) between 5850 and 6720 cm^{-1} , with a particular emphasis on intensity measurements, (ii) construction of an accurate line list for D_2 up to 24000 cm^{-1} based on the most advanced theoretical calculations. The experimental values will be compared to the theoretical results and to previous intensity measurements by Integrated Cavity Output Spectroscopy (ICOS) [14].

The report is organized as follows. After the description of the CRDS experimental setup (Section 2), we present in Section 3 the line profile analysis together with the derivation of the position, intensity and pressure shift of the observed (2-0) transitions. Section 4 is devoted to the calculation of the theoretical list while in Section 5, the agreement between experiment and theory is discussed.

2. EXPERIMENT DETAILS

The very weak electric quadrupole transitions of the first overtone band of D₂ were studied by high sensitivity CW-Cavity Ring Down Spectroscopy. The $\nu=2-0$ band is centered at about 5868 cm⁻¹. The electric quadrupole transitions of D₂ form *O*, *Q* and *S* branches corresponding to $\Delta J = -2, 0$ and $+2$, respectively. The two first transitions of the *Q* branch and the entire *S* branch are located in the spectral range accessible with our set of fibered distributed feedback (DFB) lasers (5850-7920 cm⁻¹). The D₂ transitions were searched on the basis of their line center calculated from the *ab initio* energy levels (see Section 4). In addition to *Q*(1) and *Q*(2) transitions, nine transitions of the *S* branch (*S*(0)-*S*(8)) could be measured line by line. The four strongest *S* transitions (*S*(0)-*S*(3)) were previously reported by Gupta et al. [14] while a value of the centre of the two *Q* lines was estimated from electric field induced spectra [4]. The *S*(4)-*S*(8) newly detected transitions are the weakest D₂ lines reported so far.

The fibered DFB laser CW-CRDS spectrometer used for the recordings has been described in detail in Refs. [24-26]. The electro-polished stainless steel ring down cell ($l=1.42$ m, inner diameter $\Phi=11$ mm) was fitted by a pair of super-mirrors. A single set of highly reflective mirrors was used for all the recordings. The reflectivity of the mirrors in the studied region corresponds to empty cell ring down times varying from 120 to 700 μ s. About 30 ring down events were averaged for each spectral data point. Each DFB laser diode has a typical tuning range of about 30 cm⁻¹ by temperature tuning from -10°C to 60°C. A 2 cm⁻¹ spectral section was scanned at a spectral resolution of about 2×10^{-3} cm⁻¹ (60 MHz) around each D₂ line. The achieved noise equivalent absorption (NEA), α_{min} , is on the order of 3×10^{-11} cm⁻¹.

It is possible to further decrease the noise level by averaging spectra recorded successively [27-29]. This approach was first applied to the detection of the extremely weak $a^1\Delta_g(0) - X^3\Sigma_g^-(1)$ hot band of O₂ near 1.58 μ m (NEA $\sim 2 \times 10^{-11}$ cm⁻¹ at that time) [27].

Presently, a 2 hours averaging was needed to detect the weakest *S*(8) line. 41 spectra having a $\sim 3 \times 10^{-11}$ cm⁻¹ NEA were coadded, leading to a final NEA of 4×10^{-12} cm⁻¹ in

agreement to the expected value for a Gaussian distribution of the noise. **Fig. 1** shows the $S(8)$ line located on the far wing of a line of water present as an impurity in the sample. Note that a NEA value of $\alpha_{min} = 4 \times 10^{-12} \text{ cm}^{-1}$ corresponds to a 1% decrease of the light intensity after an absorption path length of 25000 km. The $S(8)$ line has an intensity on the order of $1.8 \times 10^{-31} \text{ cm/molecule}$ at 296 K which is one of the smallest intensities ever measured in an absorption measurement [27-29].

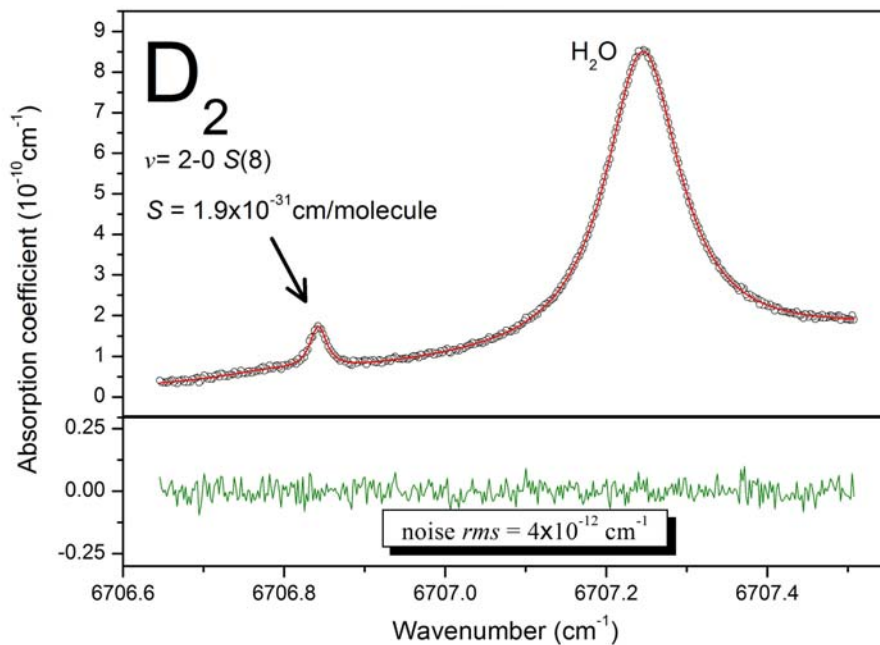


Fig. 1

The isotopic (atomic) purity of the D_2 sample (purchased from ISOTECH) was stated to be better than 99.96 %. The pressure measured by a capacitance gauge (MKS 1000 Torr full range with 0.1% stated accuracy) and the ring down cell temperature ($T = 296 \pm 1 \text{ K}$) measured by a thermo sensor (TSic 501) were monitored during the recordings. Most of the spectra were recorded with pressure values of 100.0, 250.0 and 500.0 Torr except for the $S(4)$ line for which a series of recordings was performed for pressure values ranging between 10 and 750 Torr.

Each 2 cm^{-1} wide piece of spectrum was calibrated independently on the basis of the wavelength values provided by a Fizeau type wavemeter (WSU-30 Highfinesse, 5 MHz resolution and 20 MHz accuracy). The absolute calibration provided by the wavemeter is better than $1 \times 10^{-3} \text{ cm}^{-1}$ (30 MHz). The drift of the wavemeter being very slow, relative wavenumber values are about 10 times more accurate for successive spectra recorded over a short period (one hour, for instance). When possible, the calibration was checked and refined using reference line positions of water [30] present as an impurity.

3. LINE PROFILE ANALYSIS AND INTENSITY DERIVATION

The profile of hydrogen rovibrational transitions is affected by a marked Dicke narrowing increasing with the pressure [31-36]. The reduction of the width and the pressure shift of the $S(4)$ line are illustrated in **Fig. 2** where the profiles at 100 and 500 Torr are compared (the absorption coefficient at maximum was normalised to 1 for the clarity of the comparison).

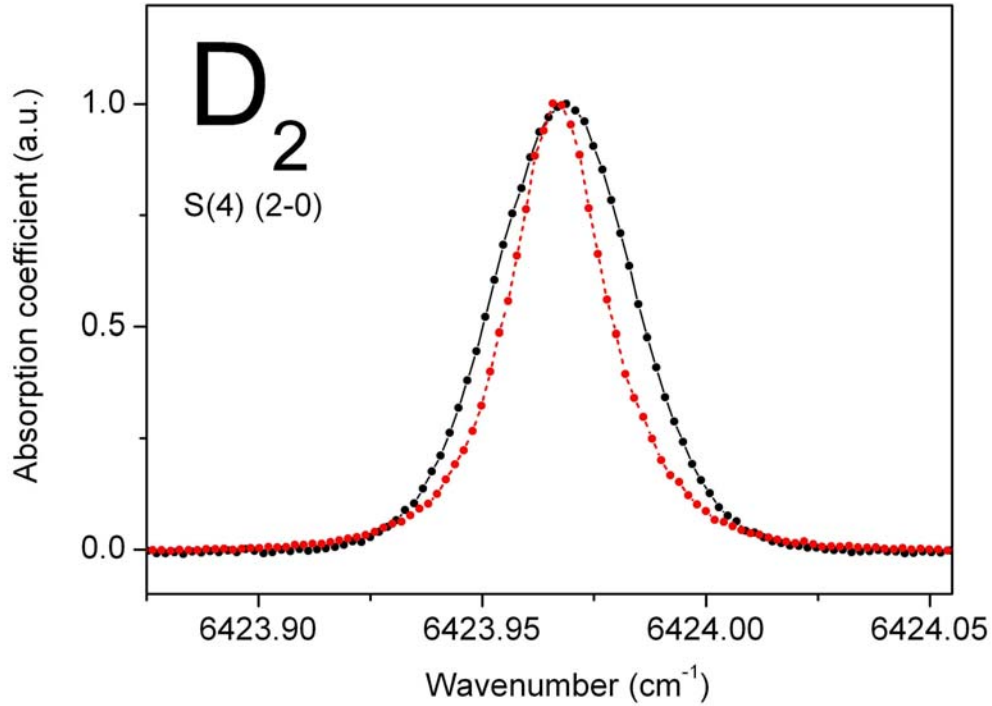


Fig. 2

The integrated absorption coefficient, A_{ν_0} ($\text{cm}^{-2}/\text{molecule}$), of a rovibrational transition centred at ν_0 (cm^{-1}), is related to the line intensity, S_{ν_0} ($\text{cm}/\text{molecule}$):

$$A_{\nu_0}(T) = \int_{\text{line}} \alpha_{\nu} d\nu = S_{\nu_0}(T)N \quad (1)$$

where ν is the wavenumber in cm^{-1} , N is the D_2 concentration in $\text{molecule}/\text{cm}^3$ obtained from the measured pressure and temperature values: $N = P/kT$, α_{ν} is the absorption coefficient in cm^{-1} obtained from the cavity ring down time, τ (in s): $\alpha = \frac{1}{c} \left(\frac{1}{\tau} - \frac{1}{\tau_0} \right)$, where c is the light velocity and τ_0 is the ring-down time of the evacuated cavity.

An interactive multi-line fitting program was used to reproduce the spectrum. In the line profile fitting, the DFB linewidth contribution (~ 2 MHz FWHM) was neglected compared to the Doppler broadening (~ 1.2 GHz FWHM). The FWHM of the Gaussian component was fixed to its theoretical value while the local baseline (assumed to be a linear function of the wavenumber), the line centre, and the integrated absorption coefficient were fitted.

The fitting of the D_2 line using a Voigt profile leads to a W shape residual which is a typical signature of Dicke narrowing effects (**Fig. 3**). The residuals presented in **Fig. 3** for the $S(4)$ and $S(6)$ lines show that a much better spectrum reproduction is obtained using a Galatry profile. A similar quality of data reproduction can be achieved with a Rautian line shape but the retrieved integrated absorption coefficient may deviate by up to 1.5 %, the Galatry values being systematically larger. The choice of the theoretical function to reproduce the measured line profile is then the main part of the overall uncertainty on the line intensity that we estimate to be 2 % for the medium and strongest lines.

As a consequence of the high sensitivity of the recordings, lines due to water were observed superimposed to several D_2 lines. (Water concentration was found to be less than 1 mTorr). The line profile fittings were performed using a Galatry profile for D_2 line and a Voigt profile for the water lines (see **Fig. 1** for instance). In the case of the extremely weak $S(8)$ line, the *rms* value of the residuals reaches the instrument noise level of $\alpha_{min} = 4 \times 10^{-12}$ cm^{-1} (**Fig. 1**).

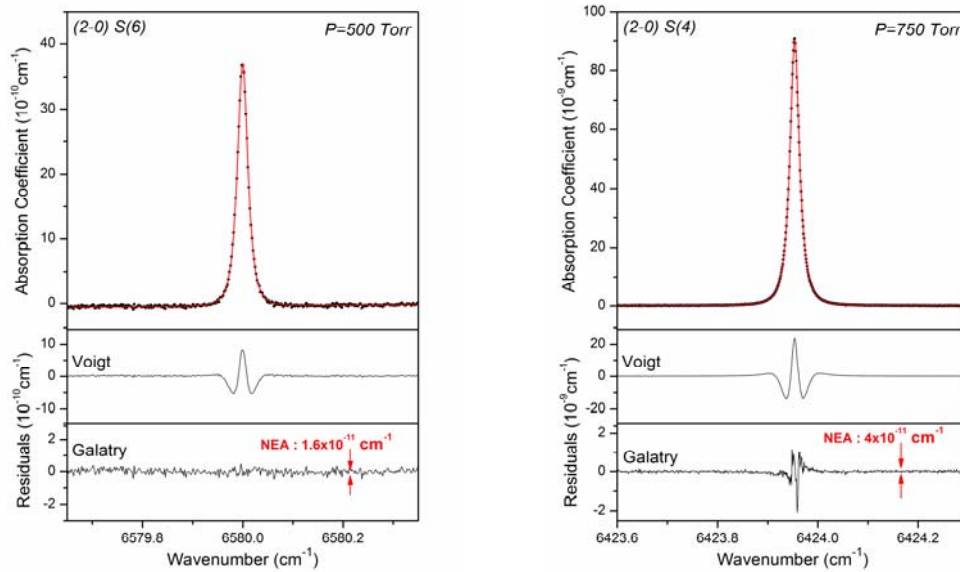


Fig. 3

Except for the $S(7)$ and $S(8)$ lines which were recorded at 600 Torr only, the other lines were studied at 100, 250 and 500 Torr in order to determine the pressure line shift. In addition, a more detailed investigation of the $S(4)$ transition was performed from a series of about twenty spectra at pressure ranging between 10 and 750 Torr.

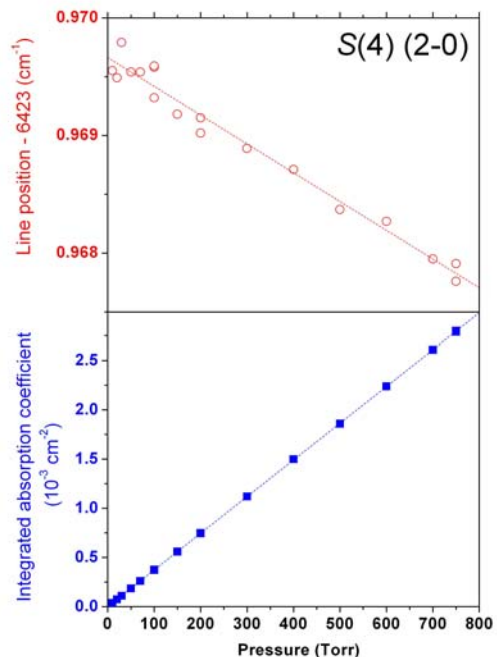


Fig. 4

The obtained position and intensity values are listed in **Table 1**. In order to increase the accuracy, the intensity of the $S(4)$ transition was computed from the proportionality factor between the integrated absorption coefficient and the pressure values (Eq. 1). **Fig. 4** shows that the linear dependence is nearly perfect (regression coefficient of 0.99999), yielding a statistical error bar of less than 1‰ on the derived slope value.

The stability of the wavemeter over the duration of a series of recordings at different pressure values makes an accurate determination of the line shifts possible. **Fig. 4** illustrates the linear variation of the centre of the $S(4)$ line with the pressure. The pressure shift values listed in **Table 1** range from -2.7×10^{-3} to -1.7×10^{-3} $\text{cm}^{-1}/\text{atm}$ at 296 K. A comparison with the values obtained by Gupta et al. [14] for the $S(0)$ - $S(3)$ lines is included in **Table 1**. The agreement is satisfactory except for the $S(3)$ line, the uncertainties claimed by Gupta et al. being significantly smaller than ours (on the order of 1% and 10 %, respectively).

In the next section, we present the construction of a theoretical line list which will be used for comparison with the obtained experimental data.

Table 1. Centre, intensity and pressure shift coefficient for the transitions of the (1-0) and (2-0) bands of D₂.

Band (ν -0)	Transition	Line position			Line intensity at 296 K			Reference
		Calc. (cm ⁻¹)	Meas. (cm ⁻¹) ^a	Shift coefficient (10 ⁻³ cm ⁻¹ / amagat)	Calc. (10 ⁻²⁸ cm/molecule)	Meas. ^c (10 ⁻²⁸ cm/molecule)	Relative difference (%) ^d	
(1-0)	S(0)	<i>3166.3605 (2)</i>	<i>3166.3620 (2)</i>	-2.5(3)	40.35	<i>37.7 (4)</i>	-6.6	<i>Maddaloni et al. 2010 [15]</i>
	S(1)	<i>3278.5231 (2)</i>	<i>3278.5220 (2)</i>	-2.0(2)	26.99	<i>27.3 (5)</i>	1.1	<i>Maddaloni et al. 2010 [15]</i>
(2-0)	Q(2)	5855.5834 (4)	5855.583 (1)	-2.16(18)	1.949	1.93 (8)	-1.0	This work
	Q(1)	5863.9371 (4)	5863.938 (1)	-2.67(12)	1.458	1.43 (4)	-1.9	This work
	S(0)	6034.6505 (4)	6034.650 (1)	-2.33(25)	3.780	3.76 (3)	-0.5	This work
			<i>6034.6498 (10)</i>	-2.169(26)		<i>3.47 (1)</i>	-8.2	<i>Gupta et al. 2007 [14]</i>
	S(1)	6140.6185 (4)	6140.620 (1)	-1.7(4)	2.774	2.75 (3)	-0.9	This work
			<i>6140.6205 (100)</i>	-1.978(92)		<i>3.35 (2)</i>	20.8	<i>Gupta et al. 2007 [14]</i>
	S(2)	6241.1277 (4)	6241.129 (1)	-2.5(5)	4.782	4.78 (6)	0.0	This work
			<i>6241.1270 (1)</i>	-1.536(28)		<i>4.36 (2)</i>	-8.8	<i>Gupta et al. 2007 [14]</i>
	S(3)	6335.7173 (4)	6335.718 (1)		1.388	1.38 (2)	-0.6	This work
			<i>6335.7168 (10)</i>	-1.805(22)		<i>1.32 (1)</i>	-4.9	<i>Gupta et al. 2007 [14]</i>
S(4)	6423.9668 (4)	6423.968 (1)	-1.859(76)	1.138	1.1453 (7)	0.6	This work	
S(5)	6505.5016 (4)	6505.502 (1) ^b	-1.8(5)	0.1686	0.177 (4)	5.0	This work	
S(6)	6579.9972 (4)	6580.002 (1)	-2.6	0.07349	0.0732 ^b	-0.4	This work	
S(7)	6647.1828 (4)	6647.186 (3) ^b		5.973E-3			This work	
S(8)	6706.8422 (4)	6706.841 (1)		1.467E-3	1.84E-3	25.4	This work	

Notes

Literature values are given in italics for comparison.

^a Value at 600 Torr

^b Highly blended with a water line

^c The uncertainty value given here is a statistical error which does not consider systematic effects as those related to the choice of the line profile function (see Text). The total uncertainty on the CRDS intensity values is on the order of 2 % for not very weak lines. The extremely small error on the S(4) intensity reflects the nearly perfect proportionality achieved between the integrated absorption coefficient and the pressure value (Fig. 4).

^d (Meas.-Calc.)/Calc.

4. THE THEORETICAL LINE LIST FOR D₂ UP TO 24000 cm⁻¹

Accurate ab initio calculations of the energy levels and quadrupole transition moments

For a long time, the most accurate and comprehensive theoretical data for both the energy levels and the quadrupole transition moments of H₂ (D₂) were those computed by Wolniewicz [18,37,38]. In a series of papers [20,21,23], some of the present coauthors (KP and JK) have performed new and more accurate *ab initio* calculations of all rovibrational levels of H₂, HD, and D₂ with a controlled uncertainty. These new results are based on perturbative treatment of the finite nuclear mass (adiabatic and nonadiabatic corrections) [39] and include relativistic and quantum electrodynamic (QED) effects. The accuracy is limited by yet unknown higher order α^4 QED corrections, and not by any numerical uncertainties. In fact the Born-Oppenheimer energies are obtained with about 10⁻¹⁴ accuracy [40], thanks to the development of analytic formulae for two-electron two-center integrals with Slater functions [41]. Presently, unknown higher order QED corrections are a bottle-neck for a further improvement in theoretical accuracy. Except for H₂⁺, they have not yet been considered in the literature for molecular systems.

Here we give more details on nonrelativistic wave function, as it will be used further for calculation of the electric quadrupole moment. The nonrelativistic wave function is a solution of the Schrödinger equation $H\Psi=E\Psi$. To solve this equation we first assume the adiabatic approximation in which the total wave function is represented by a product of the electronic and the nuclear wave functions $\Psi(r,R) = \varphi(r) \chi(R)$. The electronic wave function is an eigenfunction of the electronic (clamped nuclei) Hamiltonian H_{el} , whereas the nuclear function $\chi(R) = Y(\theta,\varphi) \chi_J(R)$, after separation of the angular variables in the spherical harmonic $Y(\theta,\varphi)$, is the solution to the radial nuclear Schrödinger equation. Adiabatic and nonadiabatic corrections are calculated using nonadiabatic perturbation theory (NAPT) [39]. With accuracy of $O(m_e/M)^2$, the rovibrational energies can be obtained from the so called nonadiabatic nuclear equation:

$$\left[-\frac{1}{R^2} \frac{\partial}{\partial R} \frac{R^2}{2\mu_{\parallel}(R)} \frac{\partial}{\partial R} + \frac{J(J+1)}{2\mu_{\perp}(R)R^2} + Y(R) \right] \chi_J(R) = E_{NR} \chi_J(R) \quad (2)$$

Here $Y(R)=E_{BO}(R)+E_{AD}(R)+E_{NA}(R)$ is a nonadiabatic interaction potential composed of the Born-Oppenheimer potential augmented by adiabatic and nonadiabatic corrections. The two functions $\mu_{\parallel}(R)$ and $\mu_{\perp}(R)$ are the R -dependent effective nuclear reduced masses. To take into account the relativistic and QED effects we extend the effective potential by further corrections:

$$Y(R) = E_{\text{BO}}(R) + E_{\text{AD}}(R) + E_{\text{NA}}(R) + E_{\text{REL}}(R) + E_{\text{QED}}(R) + E_{\text{HQED}}(R) + E_{\text{FS}}(R) \quad (3)$$

These corrections represent the electronic expectation value of the Breit-Pauli Hamiltonian, E_{REL} , the leading E_{QED} and the higher order (E_{HQED}) QED effects, as well as the effect of the finite size of the nuclei E_{FS} , which is not negligible at 10^{-4} cm^{-1} precision level.

The Born-Oppenheimer potential is obtained by solving the clamped nuclei equation using variational approach. The electronic wave function is represented as a linear combination of properly symmetrized two-electron basis functions, such as the James-Coolidge basis functions for short internuclear distances and the generalized Heitler-London basis functions for large distances. In order to evaluate all the corrections we applied exponentially correlated Gaussian (ECG) functions with carefully optimized nonlinear parameters. This includes the computation of the quadrupole moment function:

$$Q(R) = \frac{R^2}{2} - \frac{1}{2} \langle \varphi | \sum_i 3z_i^2 - r_i^2 | \varphi \rangle \quad (4)$$

needed for the transition moments and the line intensities. At present, we neglect the contribution to the intensity coming from the magnetic dipole transitions [42] because its impact on the intensities is below the experimental uncertainty. A more elaborate description of the methodology can be found in Refs. [13,21,39]. Ref. [21] contains the complete list of the dissociation energy of the 598 bound levels of D_2 .

In the context of the aforementioned theoretical calculations, a list of D_2 absorption transitions was constructed. Within the assumed very small intensity threshold of $1 \times 10^{-34} \text{ cm/molecule}$, the spectrum includes transition energies up to 24000 cm^{-1} . This part of the spectrum consists of 177 transitions belonging to ten $\nu=0$ ($\nu=0-9$) vibrational bands and of 24 transitions grouped in three $\nu=1$ ($\nu=1-3$) hot bands, exhibiting O , Q and S branches, according to the electric quadrupole selection rules of $\Delta J = J' - J'' = -2, 0$ and $+2$, respectively, with exclusion of forbidden $J=0$ to $J=0$ vibrational transitions. The frequencies (in cm^{-1}) of the transitions were obtained by difference of the appropriate energy levels reported in Ref. [21]. The uncertainty calculated for each transition frequency increases from a few 10^{-5} cm^{-1} for pure rotational transitions (below 1500 cm^{-1}) up to $1 \times 10^{-3} \text{ cm}^{-1}$ near 23000 cm^{-1} . The theoretical uncertainties estimated for D_2 are smaller than for H_2 [34]. This is a result of deuteron-to-proton mass ratio, which affects the magnitude of the recoil effects neglected in the calculations and, proportionally, their uncertainties. Details of the error analysis were given in Ref. [21].

The line intensities, S_{ν_0} (cm/molecule), were computed from the quadrupole transition moment, $\langle \nu'J'|Q(R)|\nu''J''\rangle$, using the following expression [43]:

$$N_0 S_{\nu_0} = 2.208 \times 10^{-15} \nu^3 P_{J''}(T) C_{J''} |\langle \nu'J'|Q(R)|\nu''J''\rangle|^2 \quad (5)$$

where: ν is the calculated wavenumber (cm^{-1}), N_0 is the Loschmidt's number (2.687×10^{19} molecules/ cm^3), $\langle \nu'J'|Q(R)|\nu''J''\rangle$ is expressed in Debye \times angstrom (10^{-8} D \cdot cm). $P_J(T)$ is the fraction of molecules in the J -th rotational level at the considered temperature T . It was calculated from $P_J(T) = g_J (2J+1) \exp(-\frac{\Delta E_J}{kT}) / Z(T)$ where g_J is the nuclear spin statistical weight, ΔE_J is the calculated value of the energy separation with respect to the ground rotational level and $Z(T)$ is the partition function: $Z(T) = \sum_J g_J (2J+1) \exp(-\frac{\Delta E_J}{kT})$.

The spin of the deuteron is 1. Hence, for the even values of the rotational quantum number J , the statistical weight $g_J = 2$ (ortho-D₂) whereas for odd values of J , the weight $g_J = 1$ (para-D₂). The rotational coefficients used in Eq. (5) are

$$C_J = \frac{3(J+1)(J+2)}{2(2J+1)(2J+3)} \text{ for a } S(J) \text{ transition,} \quad (6)$$

$$C_J = \frac{J(J+1)}{(2J-1)(2J+3)} \text{ for a } Q(J) \text{ transition,} \quad (7)$$

$$\text{and } C_J = \frac{3J(J-1)}{2(2J-1)(2J+1)} \text{ for a } O(J) \text{ transition.} \quad (8)$$

Fig. 5 shows a general graphical view of the line list contents. The strongest line of each is the $S(2)$ transition of the $\nu=1-0$ band with the intensity of 4.2×10^{-27} cm/molecule, which is about ten times weaker than the strongest H₂ transition. The energetically highest line at 23033 cm^{-1} corresponds to the $S(4)$ transition of the $\nu=9-0$ band. The list was prepared following the conventions adopted in the HITRAN database [30] and includes the calculated values of the transition frequencies and intensities, the corresponding lower state energy and Boltzmann factor, together with the quadrupole transition moment (in atomic unit) and the Einstein coefficient evaluated (in Hz) from $A = 1.120 \times 10^{-12} \nu^5 C_{J''} |\langle \nu'J'|Q|\nu''J''\rangle|^2$.

The line intensities were calculated at a reference temperature of $T = 296$ K and the intensity values are expressed in units of cm/molecule for pure D₂. The relative uncertainty on the line intensities is estimated to be below 0.1%. In **Table 2** we present a sample of the global line list limited to the transitions of the (0-0), (1-0), and (2-0) band with intensities larger than 1×10^{-30} cm/molecule. The global line list provided as Supplementary Material

[44]. In the next section, the calculated positions and intensities will be compared to the experimental values available in the literature and to the present CRDS measurements of the (2-0) transitions.

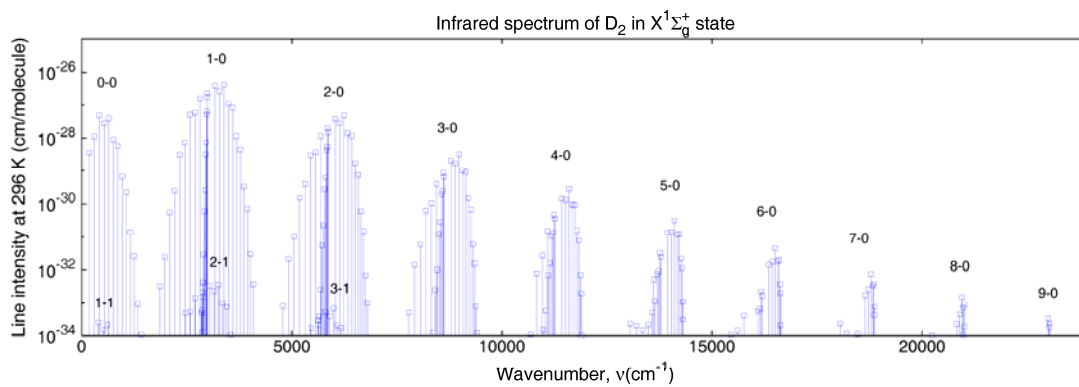


Fig. 5

Table 2. Calculated values of the position, transition moment, Einstein coefficient, lower state energy population factor and line intensity at 296 K for the (0-0), (1-0) and (2-0) transitions of D₂ with intensities larger than 1×10⁻³⁰ cm/molecule. This Table is a sample of the whole calculated line list, provided as Supplementary Material, for pure D₂ up to 24000 cm⁻¹ (intensity cut off of 1×10⁻³⁴ cm/molecule).

Band	Transition	Position (cm ⁻¹)	Transition moment $\langle v'J'Q(R)/v''J'' \rangle$ (a.u.) ^a	A (Hz)	Lower state energy (cm ⁻¹)	P_J	Intensity (cm/molecule)
(0-0)	S 0	179.067099(7)	4.7623E-01	4.6763E-12	0.0000	1.8372E-01	3.556E-29
	S 1	297.53374(1)	4.7731E-01	3.5698E-11	59.7806	2.0609E-01	1.103E-28
	S 2	414.64845(2)	4.7894E-01	1.6194E-10	179.0671	3.8470E-01	4.809E-28
	S 3	529.90025(2)	4.8110E-01	5.1574E-10	357.3144	1.1322E-01	2.760E-28
	S 4	642.80664(3)	4.8380E-01	1.3077E-09	593.7155	9.2273E-02	3.876E-28
	S 5	752.91992(3)	4.8702E-01	2.8317E-09	887.2146	1.3540E-02	8.977E-29
	S 6	859.83237(3)	4.9077E-01	5.4609E-09	1236.5222	5.8589E-03	5.744E-29
	S 7	963.18004(4)	4.9503E-01	9.6357E-09	1640.1345	4.7524E-04	6.551E-30
(1-0)	S 8	1062.64534(4)	4.9980E-01	1.5844E-08	2096.3546	1.1728E-04	2.184E-30
	O 7	2209.2735(2)	9.8840E-02	1.8605E-08	1640.1345	4.7524E-04	2.404E-30
	O 6	2329.8075(2)	9.4911E-02	2.1792E-08	1236.5222	5.8589E-03	3.122E-29
	O 5	2451.0891(2)	9.1007E-02	2.4867E-08	887.2146	1.3540E-02	7.438E-29
	O 4	2572.6450(2)	8.7131E-02	2.7376E-08	593.7155	9.2273E-02	5.066E-28
	O 3	2693.9732(2)	8.3284E-02	2.8344E-08	357.3144	1.1322E-01	5.869E-28
	O 2	2814.5500(2)	7.9469E-02	2.4984E-08	179.0671	3.8470E-01	1.610E-27
	Q 7	2935.3476(2)	7.4686E-02	3.4496E-08	1640.1345	4.7524E-04	2.525E-30
	Q 6	2949.7588(2)	7.4470E-02	3.5307E-08	1236.5222	5.8589E-03	3.155E-29
	Q 5	2962.1934(2)	7.4281E-02	3.6138E-08	887.2146	1.3540E-02	7.401E-29
	Q 4	2972.6142(2)	7.4122E-02	3.7095E-08	593.7155	9.2273E-02	5.141E-28
	Q 3	2980.9894(2)	7.3992E-02	3.8489E-08	357.3144	1.1322E-01	6.509E-28
	Q 2	2987.2934(2)	7.3894E-02	4.1566E-08	179.0671	3.8470E-01	2.378E-27
	Q 1	2991.5070(2)	7.3828E-02	5.8500E-08	59.7806	2.0609E-01	1.788E-27
	S 0	3166.3605(2)	6.8226E-02	1.6592E-07	0.0000	1.8372E-01	4.035E-27
	S 1	3278.5231(2)	6.4550E-02	1.0606E-07	59.7806	2.0609E-01	2.699E-27
	S 2	3387.2626(2)	6.0912E-02	9.5291E-08	179.0671	3.8470E-01	4.240E-27
	S 3	3492.0937(2)	5.7311E-02	9.0967E-08	357.3144	1.1322E-01	1.121E-27
(2-0)	S 4	3592.5655(2)	5.3747E-02	8.8005E-08	593.7155	9.2273E-02	8.350E-28
	S 5	3688.2676(2)	5.0219E-02	8.4928E-08	887.2146	1.3540E-02	1.122E-28
	S 6	3778.8349(2)	4.6725E-02	8.1159E-08	1236.5222	5.8589E-03	4.419E-29
	S 7	3863.9511(2)	4.3264E-02	7.6469E-08	1640.1345	4.7524E-04	3.231E-30
	O 6	5183.6726(4)	6.2097E-03	5.0864E-09	1236.5222	5.8589E-03	1.472E-30
	O 5	5313.1845(4)	6.5269E-03	6.1217E-09	887.2146	1.3540E-02	3.897E-30
	O 4	5440.9349(4)	6.8241E-03	7.1055E-09	593.7155	9.2273E-02	2.939E-29
	O 3	5566.4034(4)	7.0991E-03	7.7563E-09	357.3144	1.1322E-01	3.762E-29
	O 2	5689.0533(4)	7.3496E-03	7.2103E-09	179.0671	3.8470E-01	1.137E-28
	Q 6	5781.1602(4)	7.9294E-03	1.1575E-08	1236.5222	5.8589E-03	2.693E-30
	Q 5	5805.8170(4)	7.8555E-03	1.1690E-08	887.2146	1.3540E-02	6.232E-30
	Q 4	5826.4792(4)	7.7940E-03	1.1865E-08	593.7155	9.2273E-02	4.280E-29
	Q 3	5843.0847(4)	7.7447E-03	1.2201E-08	357.3144	1.1322E-01	5.370E-29
	Q 2	5855.5834(4)	7.7077E-03	1.3087E-08	179.0671	3.8470E-01	1.949E-28
	Q 1	5863.9371(4)	7.6830E-03	1.8334E-08	59.7806	2.0609E-01	1.458E-28
	S 0	6034.6505(4)	7.9366E-03	5.6458E-08	0.0000	1.8372E-01	3.780E-28
	S 1	6140.6185(4)	8.0732E-03	3.8239E-08	59.7806	2.0609E-01	2.774E-28
	S 2	6241.1277(4)	8.1790E-03	3.6486E-08	179.0671	3.8470E-01	4.782E-28
S 3	6335.7173(4)	8.2537E-03	3.7090E-08	357.3144	1.1322E-01	1.388E-28	
S 4	6423.9668(4)	8.2972E-03	3.8341E-08	593.7155	9.2273E-02	1.138E-28	
S 5	6505.5016(4)	8.3099E-03	3.9701E-08	887.2146	1.3540E-02	1.686E-29	
S 6	6579.9972(4)	8.2922E-03	4.0918E-08	1236.5222	5.8589E-03	7.349E-30	

^a To convert from atomic unit (a.u.) to Debye multiply by 2.541 746 23 Debye/a.u.

5. DISCUSSION

Overview of the literature observations

The observations of D₂ transitions from absorption spectra are much more limited than those of the main isotopologue, H₂. As reviewed in Ref. [34], overall 39 transitions of H₂ ranging from the *S*(0) pure rotational line near 354 cm⁻¹ up to the *S*(1) transition of the (5-0) band near 18908 cm⁻¹ were reported in the literature. In the case of the D₂ species, the observations do not extend beyond the first overtone band centered at 5868 cm⁻¹. This situation results from the fact that D₂ transitions are significantly weaker than H₂ transitions and that the amount of gas required for filling very long multipass cells as those used for the H₂ measurements is a limitation in the case of D₂. An extensive investigation by electric field induced absorption is due to Brannon et al. [4] who measured the positions of thirteen $\nu=1-0$ lines and the *Q*(0)-*Q*(2) lines of the $\nu=2-0$ band with an accuracy ranging between 0.02 and 0.08 cm⁻¹. In 1978, McKellar and Oka [3] used a multipass cell (absorption path length in the range 64-80 m) and a frequency modulation of an infrared difference frequency laser system to measure the positions of the *O*(2)-*O*(4), *Q*(1)-*Q*(4) and *S*(0)-*S*(3) lines of the fundamental band. The positions were reported with an uncertainty on the order of 4×10⁻⁴ cm⁻¹ but no intensity information was provided [3]. Only recently, the line intensities of six D₂ transitions have become available: (i) Maddaloni et al. [15] used CW-CRDS to measure the *S*(0) and *S*(1) transitions of the fundamental band near 3 μm and reported position values with a 2×10⁻⁴ cm⁻¹ uncertainty (ii) the *S*(0)-*S*(3) transitions of the first overtone band were studied by Gupta et al. using Integrated Cavity Output Spectroscopy (ICOS) with a single mode DFB diode laser (*P*<900 Torr) [14].

More observations of D₂ transitions were performed by spontaneous Raman spectroscopy [5-12]. In particular Jennings et al. [8] measured the *S*(0)-*S*(6) rotational transitions and nine transitions of the fundamental band by laser Raman spectroscopy. By using diffusion flames of D₂ burning in air, they could extend the Raman observations of the rotational lines up to *S*(12) [9]. The review of the positions of the $\nu=0-0$ and $\nu=1-0$ transitions included in Refs. [3, 9], shows that the best determinations of the Raman positions are on the order of a few 10⁻³ cm⁻¹ for the rotational lines and 2×10⁻² cm⁻¹ for the $\nu=1-0$ transitions. Additional line positions extending up to the *Q* branch of the $\nu=2-0$ band were measured by Veirs and Rosenblatt with an estimated uncertainty ranging between ±0.03 and ±0.1 cm⁻¹ [12].

In summary, literature provides accurate position measurements only for transitions of the $\nu=0-0$ [8], $1-0$ [3,8,15] and $2-0$ [14] bands. Intensity information is limited to the $\nu=1-0$ $S(0)$ and $S(1)$ [15] and $\nu=2-0$ $S(0)$ - $S(3)$ transitions [14] which are highlighted on the calculated spectrum of **Fig. 6**, together with present CRDS measurements of the $\nu=2-0$ band.

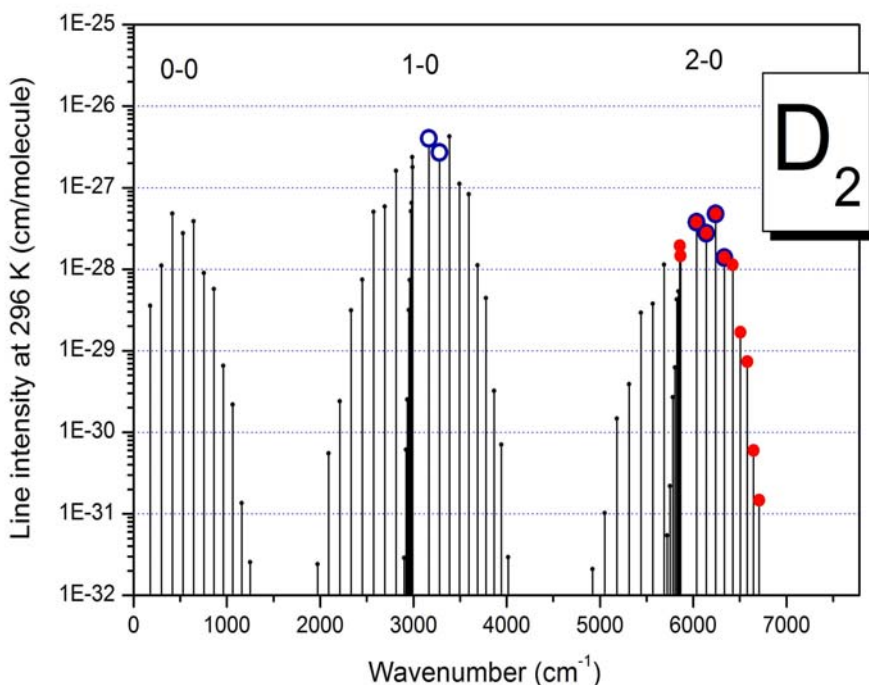


Fig.6

Line positions

The reader is referred to Ref. [21] for a quantitative comparison of the calculated transition wavenumbers to most of the published experimental values mentioned above. An overall agreement within the experimental uncertainties was noted for the $\nu=0-0$ and $\nu=1-0$ transitions obtained by Jennings et al. [8] and McKellar and Oka [3]. Nevertheless, deviations by seven and five experimental uncertainties of the recent $S(0)$ and $S(1)$ positions of the fundamental band reported by Maddaloni et al. [15] remain unexplained. Ref. [21] includes also the comparison for the ground level dissociation energy and the energy separation of the two first rotational levels recently determined with a $9.5 \times 10^{-4} \text{ cm}^{-1}$ accuracy from highly accurate measurements of the ionization energies of ortho- and para- D_2 [16]. The theory-experiment difference amounts to $5(11) \times 10^{-4} \text{ cm}^{-1}$ for D_0 and $-6.8(9.5) \times 10^{-4} \text{ cm}^{-1}$ for the para-ortho energy separation which illustrates the level of accuracy achieved in the calculations. The experimental and calculated results of the eleven $\nu=2-0$ positions measured by CRDS agree within their combined uncertainty ($1 \times 10^{-3} \text{ cm}^{-1}$ and $4 \times 10^{-4} \text{ cm}^{-1}$, respectively). The

same applies for the $\nu= 2-0$ $S(0)$ - $S(3)$ transitions measured by Gupta et al. [14] with uncertainties ranging between 1×10^{-4} to 1×10^{-2} cm^{-1} (see Table 1).

We provide in **Table 3** the vibrational term and rotational constants for the $\nu= 0-19$ vibrational states, obtained from the fit of the $J=0-7$ calculated rotational levels [21]. The usual expression of the vibration-rotational energy levels was used to fit the theoretical values: $F_\nu(J) = G_\nu + B_\nu J(J+1) - D_\nu J^2(J+1)^2 + H_\nu J^3(J+1)^3$ where G_ν is the vibrational term value, B_ν is the rotational constant, D_ν and H_ν are centrifugal distortion constants. We note that the *rms* of the fit remains limited to $2-3 \times 10^{-4}$ cm^{-1} up to very high vibrational levels, this value being significantly smaller than the uncertainty on the theoretical values of the energy levels. Nevertheless, the expansion being limited to the first distortion terms, the obtained parameters are not expected to reproduce with the same accuracy the higher energy levels.

Table 3.

Rovibrational parameters of the $\nu=0-19$ vibrational levels of D_2 obtained from the fit of the $J=0-7$ energy levels calculated in Ref. [21].

ν	$E_\nu(\text{cm}^{-1})$	$B_\nu(\text{cm}^{-1})$	$D_\nu(10^{-2} \text{cm}^{-1})$	$H_\nu(10^{-6} \text{cm}^{-1})$	<i>rms</i> (10^{-4}cm^{-1})
0	0.0(00)	29.913163(30)	-1.14837(16)	5.753(21)	2.36
1	2993.61728(21)	28.857553(43)	-1.12095(20)	5.667(23)	2.09
2	5868.12064(22)	27.820413(45)	-1.09465(21)	5.585(25)	2.20
3	8625.60212(22)	26.798198(46)	-1.06940(21)	5.499(25)	2.23
4	11267.71502(22)	25.787207(46)	-1.04527(21)	5.410(25)	2.22
5	13795.65220(23)	24.783428(47)	-1.02226(22)	5.307(26)	2.29
6	16210.11569(22)	23.782543(45)	-1.00061(21)	5.199(24)	2.17
7	18511.27678(21)	22.779703(43)	-0.98047(20)	5.087(24)	2.11
8	20698.72310(22)	21.769463(45)	-0.96201(20)	4.961(24)	2.16
9	22771.39141(22)	20.745571(45)	-0.94555(20)	4.819(24)	2.16
10	24727.48172(21)	19.700785(42)	-0.93162(19)	4.670(23)	2.06
11	26564.34831(21)	18.626462(43)	-0.92069(20)	4.491(24)	2.10
12	28278.36103(22)	17.512254(44)	-0.91362(20)	4.279(24)	2.14
13	29864.72882(24)	16.345454(50)	-0.91164(23)	4.018(27)	2.41
14	31317.27304(24)	15.110176(48)	-0.91652(22)	3.678(26)	2.35
15	32628.13477(26)	13.786093(53)	-0.93089(24)	3.195(29)	2.58
16	33787.39269(31)	12.346516(63)	-0.95930(29)	2.466(34)	3.07
17	34782.56031(39)	10.754923(80)	-1.00925(37)	1.195(44)	3.90
18	35597.91551(77)	8.95867(16)	-1.09536(73)	-1.478(86)	7.70
19	36213.6318(29)	6.87414(60)	-1.2473(28)	-9.72(33)	2.92

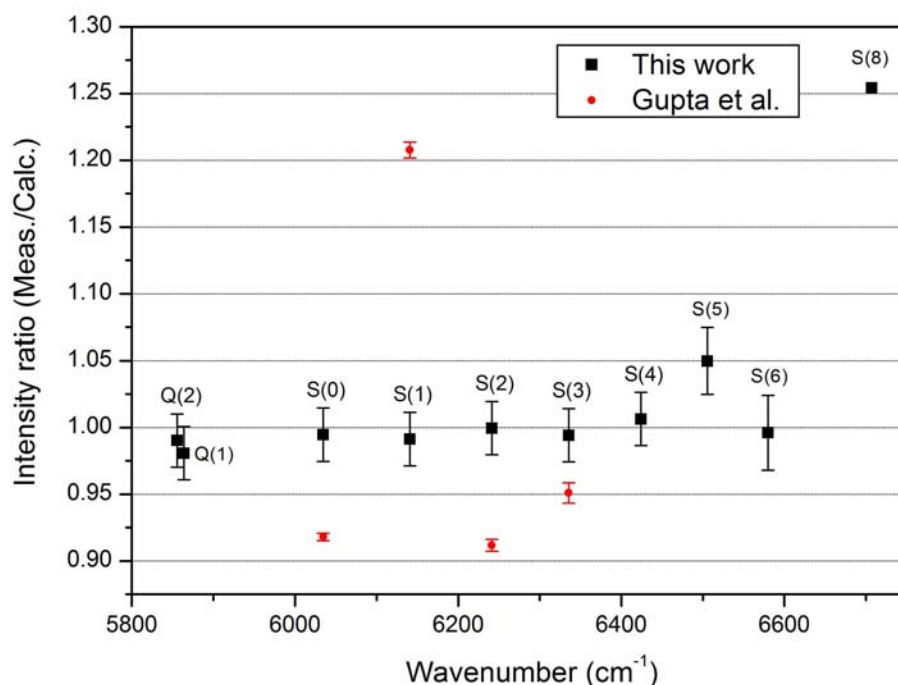
Note

The uncertainties are given in parenthesis in the unit of the last quoted digit. They correspond to the statistical error of the fit and do not take into account the error bar on the calculated value of the energy levels.

Line intensities

The available values of D_2 line intensities are gathered in Table 1 together with the corresponding relative deviation from the calculated values. The $\nu= 1-0$ $S(0)$ and $S(1)$

intensities deviate by -6.6% and 1.1%, the claimed experimental uncertainty being on the order of 1 % and 2 %, respectively [15]. **Fig. 7** shows the relative difference, (meas./calc.-1), for the $\nu=2-0$ transitions measured by CRDS and ICOS [14]. If we except the highly blended $S(5)$ line and the extremely weak $S(8)$ transition, the deviations range between -1.9 and +0.6 % for the CRDS data, the deviations being much larger (up to 21 %) for the ICOS measurements [14]. A possible explanation for the large underestimation of the $S(0)$, $S(2)$ and $S(3)$ ICOS intensities is that Gupta et al. [14] used a Voigt profile to reproduce their experimental line profile while Dicke narrowing effects are strong in hydrogen transitions. In Ref. [33], the HD intensity values obtained from the simulations performed with a Voigt profile or a Rautian profile were compared; a difference increasing with the pressure up to 8% at 750 Torr was evidenced, the Voigt profile leading to smaller values than the Rautian profile (see Fig. 4 of Ref. [33]).



6. CONCLUSION

Eleven electric quadrupole transitions of the first overtone band of D₂ have been measured by very high sensitivity CW-Cavity Ring Down Spectroscopy (CRDS) between 5850 and 6720 cm⁻¹. They include the weakest and the most excited D₂ transitions reported so far by absorption spectroscopy. In particular, noise equivalent absorption on the order of $\alpha_{min} \approx 4 \times 10^{-12}$ cm⁻¹ was necessary to detect the S(8) transition which is among the weakest transitions ever reported from laboratory experiments (line intensity on the order of 1.8×10^{-31} cm/molecule). A Galatry profile was used to derive the positions, strengths and pressure shift coefficients.

On the basis of the most advanced theoretical calculations [21], we have constructed a highly accurate and complete theoretical line list for pure D₂ (0 - 24000 cm⁻¹, intensity cut off of 1×10^{-34} cm/molecule). The comparison between the CRDS and theoretical results shows an agreement within the claimed experimental uncertainty for both position and intensities. The uncertainty on the experimental intensities is mainly limited by the choice of the theoretical expression adopted to fit the measured line profile. The conservative value of 2% estimated for the CRDS line intensities is at least one order of magnitude larger than the accuracy claimed for the calculated intensities. The measurement of line positions provides a more accessible way to test the *ab initio* results. The accuracy of the present position measurements does not reach the theoretical uncertainties (on the order of 4×10^{-4} cm⁻¹ for the $\nu = 2-0$ band) but a better position accuracy can be reached by using highly accurate reference line positions or frequency comb assisted frequency measurements. For instance, the $\nu = 3-0$ S(3) position of H₂ has been recently measured with a 1.6 MHz accuracy (5×10^{-5} cm⁻¹) about 50 times better than the claimed theoretical accuracy [36], providing a new challenge for the calculations of the combined nonadiabatic-relativistic and quantum electrodynamic contributions to the rovibrational energy levels.

Overall, no obvious discrepancy between experiments and theoretical calculations of Ref. [21] has been identified neither for the main isotopologue H₂ [34], nor for HD [33] and D₂. However, a few experimental results deviate by a value largely exceeding the claimed experimental uncertainties (it is for instance the case of the S(0) and S(1) positions of the fundamental band of D₂ reported in Ref. [15]). In such situations, a confirmation of the experimental results by additional experiments is desirable in order to exclude possible bias. For instance, while several previous works have reported important deviations between

calculated and experimental intensities of the (3-0) transitions of H₂, a very good agreement has been recently achieved from new highly sensitive CRDS measurements [36].

Acknowledgements

J.K. acknowledges the support of the Polish Ministry of Science and Higher Education *via* Grant No. N N204 015338. Part of the computations has been performed within a computing grant from Poznań Supercomputing and Networking Center.

Figure Captions

Fig. 1.

Detection of the extremely weak $S(8)$ line of D_2 .

Upper panel: CRDS spectrum of D_2 recorded at 700 Torr. The $\nu=2-0$ $S(8)$ line of D_2 is located in the far wing of a line of water present as an impurity in the CRDS cell. The dots correspond to the measurements while the solid line is the line profile simulation obtained with a Galatry profile for D_2 and a Voigt profile for H_2O .

Lower panel: Residuals between the experimental and simulated spectra. The *rms* of the residuals is close to the noise equivalent absorption ($\alpha_{\min} \approx 4 \times 10^{-12} \text{ cm}^{-1}$).

Fig. 2.

Comparison of the profile of the $\nu=2-0$ $S(8)$ line of D_2 recorded at 100 and 500 Torr. (solid and dot lines, respectively) showing the Dicke narrowing effect and the pressure induced line shift. The absorption coefficient at maximum has been normalised to 1 for the clarity of the comparison.

Fig. 3.

Line profile simulation of the $\nu=2-0$ $S(6)$ and $S(4)$ lines of D_2 recorded at 500 Torr and 750 Torr, respectively.

Upper panels: Experimental spectrum (dots) and profile simulation using a Galatry profile (red line).

Lower panels: Residuals between the experimental and simulated spectra for the Voigt, and Galatry profiles. Note the different scale used for the residuals.

Fig. 4.

Line intensity and pressure shift retrievals for the $\nu=2-0$ $S(4)$ transition of D_2 .

Upper panel: Variation of the line centre versus the pressure and corresponding linear fit;

Lower panel: Variation of the integrated absorption coefficient at 296K obtained with a Galatry profile fit versus the pressure. The straight lines correspond to the best linear fit (regression coefficient of 0.99999).

Fig. 5.

Overview of the calculated spectrum of D_2 at 296 K between 0 and 24000 cm^{-1} . Note that a number of hot band transitions contribute to the spectrum below 7000 cm^{-1} .

Fig. 6.

Overview of the calculated spectrum of D_2 at 296 K. The D_2 transitions reported in the literature with intensity values [14, 15] are highlighted (open circles blue) together with the present CRDS measurements (full circles red).

Fig. 7.

Intensity ratio at 296 K for the (2-0) transitions versus the calculated intensity values. The squares and stars correspond to the CRDS (this work) and ICOS [14] measurements, respectively. The error bars are those given in Ref. [14] for the ICOS measurements while a constant value of 2% is adopted for the strongest CRDS values, mostly related to the choice of the line profile function (see Text). The uncertainty on the temperature value (296 \pm 1 K) contributes slightly to the uncertainty on the CRDS intensities of the $S(4)$ - $S(6)$ lines.

References

- 1 T. F. Anderson and D. M. Yost, *J. Chem. Phys.* **3**, 242 (1935).
- 2 G. K. Teal and G. E. MacWood, *J. Chem. Phys.* **3**, 760 (1935).
- 3 A. R. W. McKellar and T. Oka, *Can. J. Phys.* **56**, 1315 (1978).
- 4 P. J. Brannon, C. H. Church, and C. W. Peters, *J. Mol. Spectrosc.* **27**, 44 (1968).
- 5 B. P. Stoicheff, *Can. J. Phys.* **35**, 730 (1957).
- 6 E. C. Looi, J. C. Stryland, and H. L. Welsh, *Can. J. Phys.* **56**, 1102 (1978).
- 7 M. A. Henesian, M. D. Duncan, R. L. Byer, and A. D. May, *Opt. Lett.* **1**, 149-151 (1977).
- 8 D. E. Jennings, A. Weber, and J. W. Brault, *Applied Optics* **25**, 284 (1986).
- 9 D. E. Jennings, A. Weber, and J. W. Brault, *J. Mol. Spectrosc.* **126**, 19 (1987).
- 10 E. C. Looi, J. C. Stryland, and H. L. Welsh, *Can. J. Phys.* **56**, 1102 (1978).
- 11 M. A. Henesian, M. D. Duncan, R. L. Byer, and A. D. May, *Opt. Lett.* **1**, 149 (1977).
- 12 D. K. Veirs and G. M. Rosenblatt, *J. Mol. Spectrosc.* **121**, 401 (1987).
- 13 H. Bredohl and G. Herzberg, *Can. J. Phys.* **51**, 867 (1973).
- 14 M. Gupta, T. Owano, D. S. Baer, and A. O'Keefe, *Chem. Phys. Lett.* **441**, 204 (2007).
- 15 P. Maddaloni, P. Malara, E. De Tommasi, M. De Rosa, I. Ricciardi, G. Gagliardi, F. Tamassia, G. Di
16 Lonardo, and P. De Natale, *J. Chem. Phys.* **133**, 154317 (2010).
- 17 J. Liu,, D. Sprecher, C. Jungen, W. Ubachs, and F. Merkt, *J. Chem. Phys.* **132**, 154301 (2010).
- 18 H. M. James and A. S. Coolidge, *J. Chem. Phys.* **1**, 825 (1933).
- 19 L. Wolniewicz, I. Simbotin, and A. Dalgarno, *Astrophys. J., Suppl. Ser.* **115**, 293(1998).
- 20 W. Kolos and L. Wolniewicz, *J. Chem. Phys.* **43**, 2429 (1965).
- 21 K. Piszczatowski, G. Łach, M. Przybytek, J. Komasa, K. Pachucki, and B. Jeziorski, *J. Chem. Theory
Comput.* **5**, 3039 (2009).
- 22 J. Komasa, K. Piszczatowski, G. Łach, M. Przybytek, B. Jeziorski, and K. Pachucki, *J. Chem. Theory
Comput.* **7**, 3105 (2011).
- 23 B. J. Drouin, S. Yu, J. C. Pearson, and H. Gupta, *J. Mol. Struct.* **1006**, 2 (2011).
- 24 K. Pachucki and J. Komasa, *Phys. Chem. Chem. Phys.* **12**, 9188 (2010).
- 25 J. Morville, D. Romanini, A.A. Kachanov, and M. Chenevier, *Appl. Phys.* **D78**, 465 (2004).
- 26 P. Macko, D. Romanini, S.N. Mikhailenko, O.V. Naumenko, S. Kassı, A. Jenouvrier, VI.G. Tyuterev
and A. Campargue, *J. Mol. Spectrosc.* **227**, 90 (2004).
- 27 B.V. Perevalov, S. Kassı, D. Romanini, V.I. Perevalov, S.A. Tashkun, and A. Campargue, *J. Mol.
Spectrosc.* **238**, 241 (2006).
- 28 S. Kassı, D. Romanini, A. Campargue and B. Bussery-Honvault, *Chem. Phys. Letters* **409**, 281 (2005).
- 29 H. Huang and K. K. Lehmann, *Applied Optics* **49**, 1378 (2010).
- 30 D. A. Long, D. K. Havey, M. Okumura, H. M. Pickett, C. E Miller, and J.T.Hodges, *Phys. Rev. A.* **80**
042513 (2009).
- 31 L.S. Rothman, I.E. Gordon, A. Barbe, D. Chris Benner, P.F. Bernath, M. Birk, V. Boudon, L.R. Brown,
A. Campargue, J.-P. Champion, K. Chance, L.H. Coudert, V. Dana, V.M. Devi, S. Fally, J.-M. Flaud,
R.R. Gamache, A. Goldman, D. Jacquemart, I. Kleiner, N. Lacome, W. J. Lafferty, J.-Y. Mandin, S.T.
Massie, S.N. Mikhailenko, C.E. Miller, N. Moazzen-Ahmadi, O.V. Naumenko, A.V. Nikitin, J. Orphal,
V.I. Perevalov, A. Perrin, A. Predoi-Cross, C.P. Rinsland, M. Rotger, M. Šimečková, M.A.H. Smith, K.
Sung, S.A. Tashkun, J. Tennyson, R.A. Toth, A.C. Vandaele, and J. Vander Auwera, *J. Quant.
Spectrosc. Radiat. Transfer.* **110**, 533 (2009).
- 32 S. L. Bragg, J. W. Brault, and W. H. Smith, *Astrophys. J.* **263**, 999 (1982).
- 33 J. D. Kelley and S. L. Bragg, *Phys. Rev. A* 1986, **34**, 3003 (1986).
- 34 S. Kassı and A. Campargue, *J. Mol. Spectrosc.* **267**, 36 (2011).
- 35 A. Campargue, S. Kassı, K. Pachucki, and J. Komasa, *Phys. Chem. Chem. Phys.* **14**, 802 (2012).
- 36 S.-M. Hu, H. Pan, C.-F. Cheng, X.-F. Li, J. Wang, A. Campargue, and A.W. Liu, *Astrophys. Lett.*
doi:10.1088/0004-637X/747/1/1 (2012).
- 37 C.-F. Cheng, Y. R. Sun, H. Pan, J. Wang,, A.-W. Liu, A. Campargue, and S.-M. Hu, *Phys. Rev. A* **85**,
024501 (2012).
- 38 L. Wolniewicz, *J. Chem. Phys.* **103**, 1792 (1995).
- 39 J. L. Hunt, J. D. Poll, and L. Wolniewicz, *Can. J. Phys.* **62**, 1719 (1984).
- 40 K. Pachucki and J. Komasa, *J. Chem. Phys.* **130**, 164113 (2009).
- 41 K. Pachucki, *Phys. Rev. A* **82**, 032509 (2010).
- 42 K. Pachucki, *Phys. Rev. A* **80**, 032520 (2009).
- 43 K. Pachucki and J. Komasa, *Phys. Rev. A* **83**, 032501 (2011).
- 44 G. Karl and J. D. Poll, *J. Chem. Phys.* **46**, 2944 (1967).
- 45 See Supplementary Material Document No. _____ for the calculated line list.

Fig.1

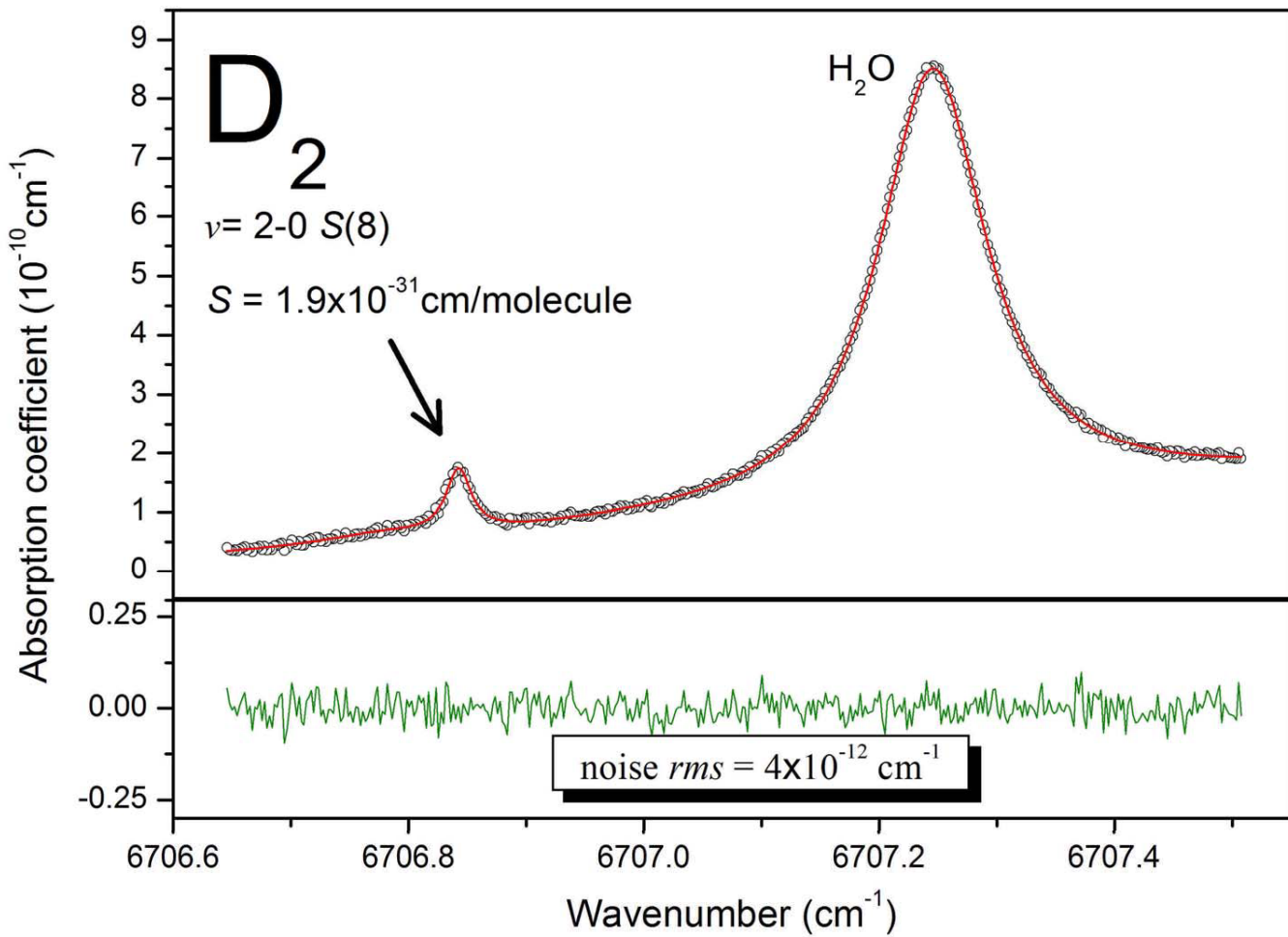


Fig. 2

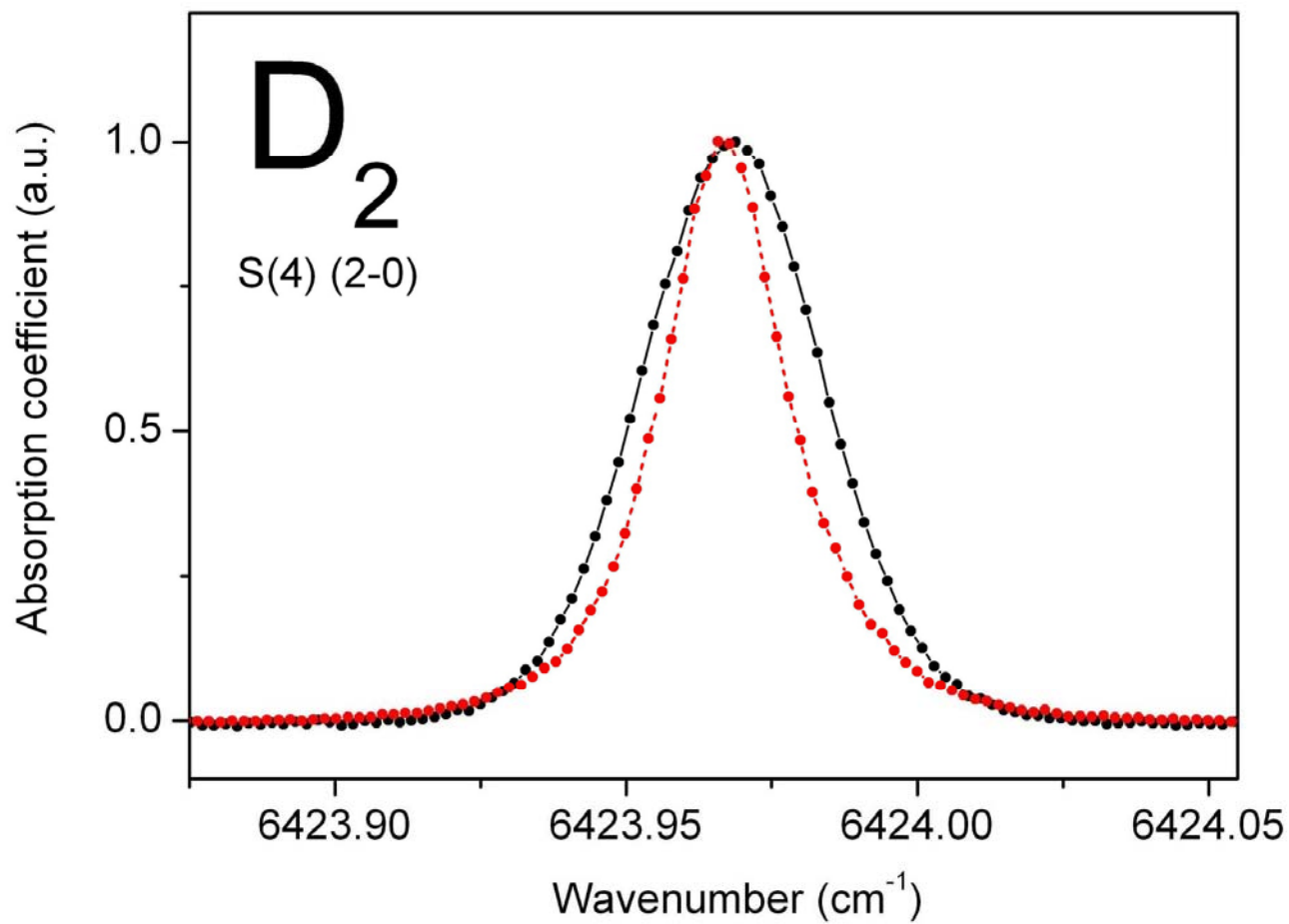
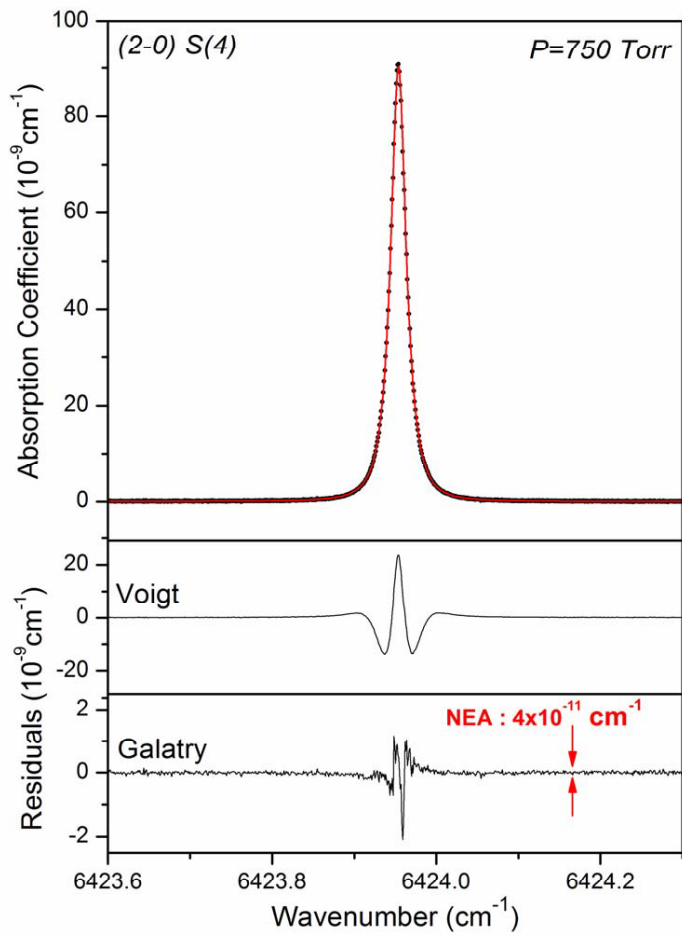
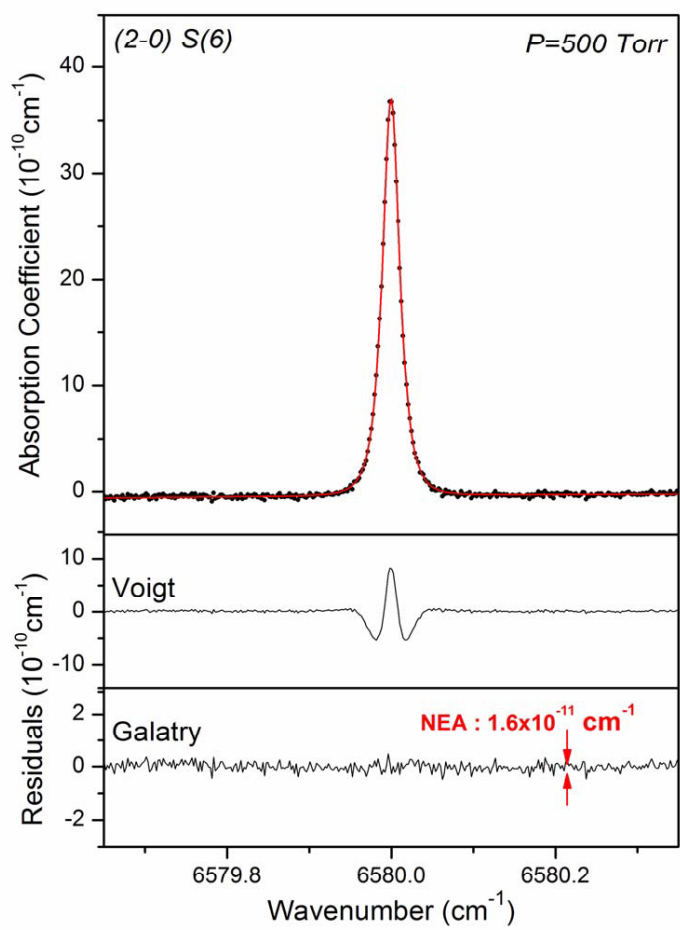


Fig.3



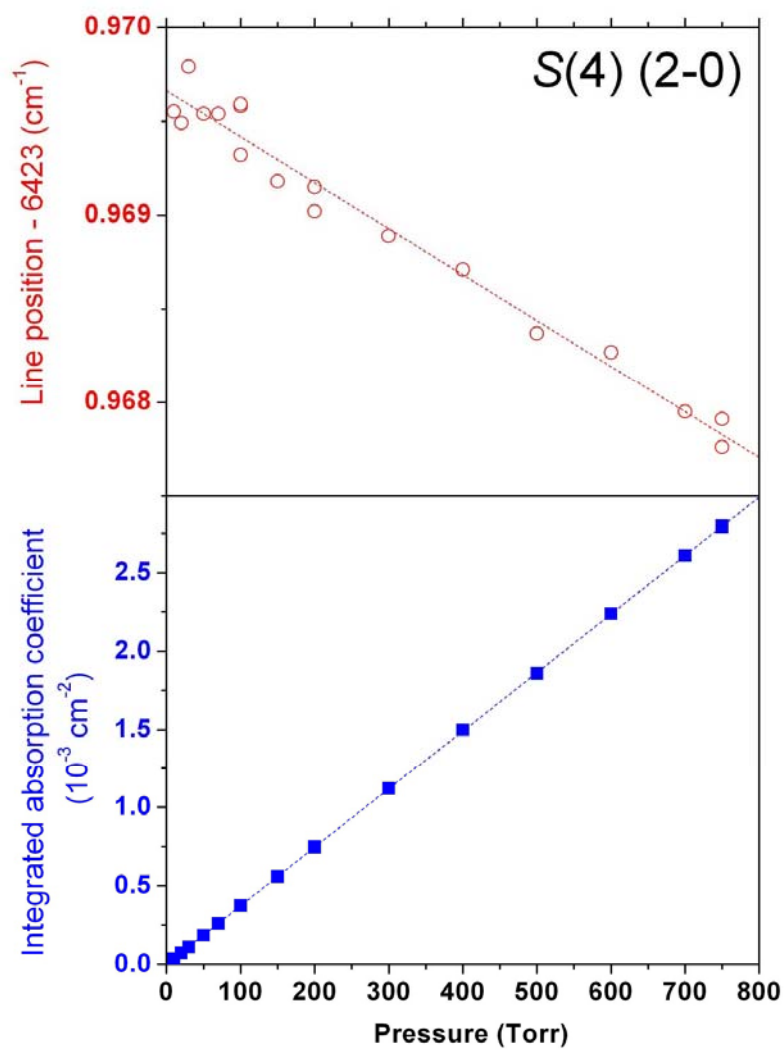


Fig.4

Fig.5

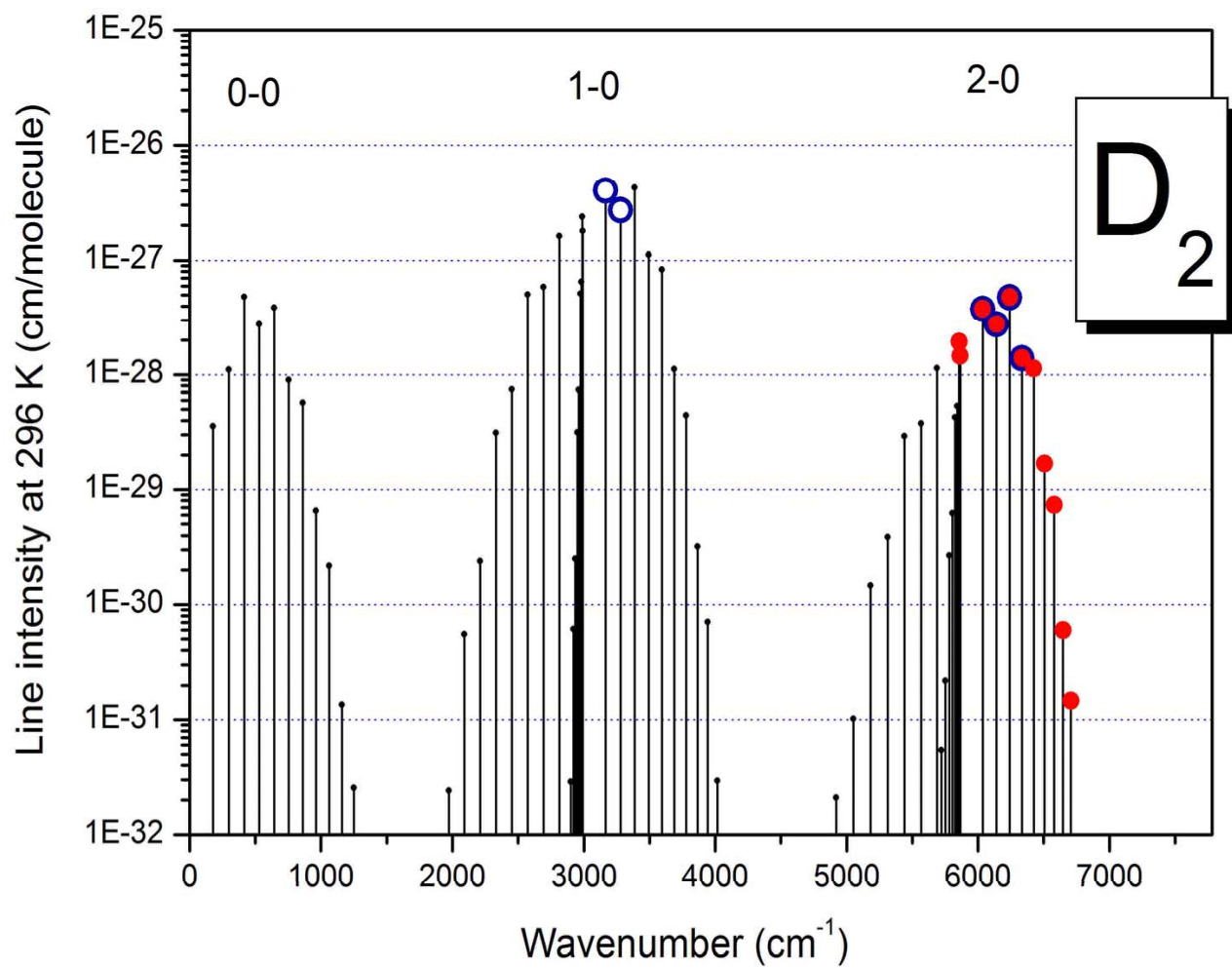


Fig.6

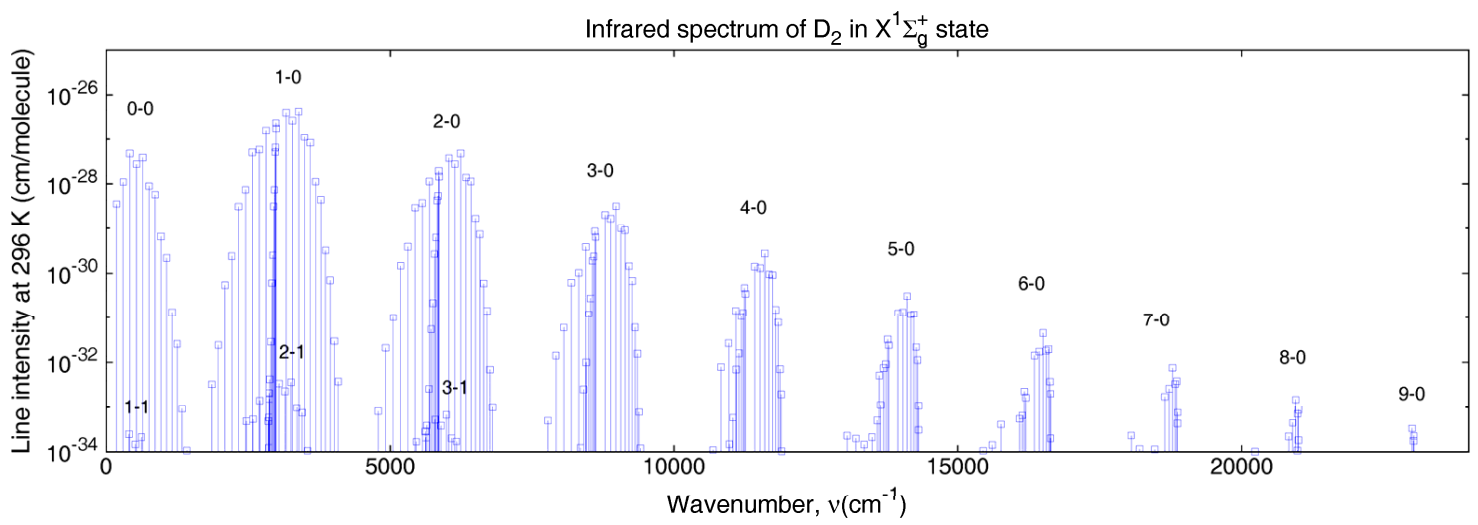


Fig.7

